J Therm Anal Calorim (2016) 123:2523–2530
DOI 10.1007/s10973-015-5228-2

Solid-state thermal and spectroscopic studies of the anti-inflammatory drug sulindac using UV–Vis, MIR, NIR, DSC, simultaneous TG–DSC, and the coupled techniques TG-EGA-MIR and DSC–optical microscopy

Renan B. Guerra[1] · **Diogo A. Gálico**[1] · **Bruno B. C. Holanda**[1] · **Gilbert Bannach**[1]

Received: 10 June 2015 / Accepted: 22 December 2015 / Published online: 6 January 2016

Abstract Simultaneous thermogravimetry–differential scanning calorimetry (TG–DSC), differential scanning calorimetry–optical microscopy (DSC–optical microscopy), online coupled thermogravimetry–infrared spectroscopy evolved gas analyses (TG-EGA-MIR), and spectroscopic techniques were used to study the non-steroidal anti-inflammatory drug sulindac in polymorphic form II. The TG–DSC curves, which were performed with the aid of DSC–optical microscopy, provided information concerning the thermal stability and decomposition profiles of the compound. From the TG-EGA-MIR coupled technique, it was possible to identify formaldehyde as a volatile compound that was released during thermal decomposition. A complete spectroscopic characterization in the ultraviolet, visible, near- and middle-infrared regions was performed in order to understand the spectroscopic properties of sulindac form II.

Keywords Sulindac · Thermal behavior · Spectroscopic studies · Coupled TG-EGA-MIR · DSC–optical microscopy

Introduction

Non-steroidal anti-inflammatory drugs (NSAIDs) are one of the most common classes of drugs that have analgesic, anti-inflammatory, and antipyretic properties. Sulindac, or {(1Z)-5-fluoro-2-methyl-1-[4-(methylsulfinyl)benzylidene]-1H-indene-3-yl}acetic acid (Fig. 1), is a NSAID that was first synthesized by Shen et al. [1] in 1972. It belongs to a group of heterocyclic and arylic derivatives of acetic acid, similar to indomethacin and etodolac, and works as a prodrug that undergoes a biotransformation in vivo, whose metabolites are biologically active and reduce the synthesis of prostaglandins from arachidonic acid via inhibition of the cyclooxygenase (COX) enzymes (COX-1 and COX-2) [2, 3]. Studies related to this drug have received more importance in recent years after some published works showed the potential of this anti-inflammatory in the treatment of colon [4] and lung cancer [5]. Recent studies [6, 7] have demonstrated that sulindac may induce apoptosis of cancer cells by a mechanism that is not completely understood, and there also have been studies for the application of this drug in the treatment of Alzheimer's disease [8].

Despite the increasing interest concerning this drug, few studies related to its thermal behavior are found in the literature. In previous studies, Ilarduya et al. [9] studied three polymorphic forms by thermal analysis and also three different solvates in acetone, chloroform, and benzene for sulindac drug. They reported the melting point of the three polymorphic forms of sulindac and found for form I $T_{onset} = 187$ °C and $\Delta_{fus}H = 27.4$ kJ mol^{-1}, form II $T_{onset} = 183$ °C and $\Delta_{fus}H = 29.8$ kJ mol^{-1}, and form III $T_{onset} = 145$ °C and $\Delta_{fus}H = 11$ kJ mol^{-1}. Grzesiak et al. [10] carried out studies using TG at a heating rate of 10 °C min^{-1} in nitrogen up to 220 °C to determine the presence of solvent crystal lattices, as well as DSC studies for the determination of the melting point of various polymorphic forms and reported the melting point of sulindac form II $T_{onset} = 185$ °C and $\Delta_{fus}H = 31.1$ kJ mol^{-1} and of a new polymorphic form IV of sulindac which melts at $T_{onset} = 130.8$ °C and $\Delta_{fus}H = 21.4$ kJ mol^{-1}.

Electronic supplementary material The online version of this article (doi:10.1007/s10973-015-5228-2) contains supplementary material, which is available to authorized users.

✉ Gilbert Bannach
gilbertbannach@yahoo.com.br; gilbert@fc.unesp.br

[1] Faculdade de Ciências, Departamento de Química, UNESP - Univ. Estadual Paulista, 17033-360 Bauru, São Paulo, Brazil

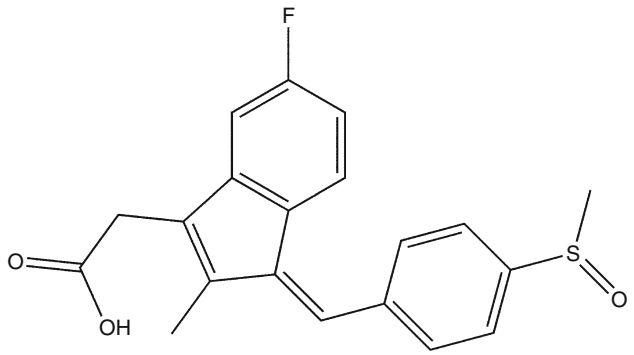

Fig. 1 Structure of sulindac

Plakogiannis and McCauley [11] determined the melting point of sulindac form I and form II to be 191 and 186 °C, respectively, and suggested that the drug melts with simultaneous decomposition. Although some studies have performed the thermal analysis of sulindac at approximately 220 °C, there are no studies regarding its thermal behavior at higher temperatures.

The physicochemical characterization of commercial drugs is important for standardization and evaluation of purity, making it suitable for the study of preformulation [12], interactions with excipients [13], decomposition kinetics [14], polymorphism [15], etc. The use of evolved gas analysis (EGA) regarding the products derived from the thermal decomposition of the active ingredients is important because these products may appear as impurities in commercial drugs [16, 17] which makes the use of coupled TG-EGA-MIR a valuable tool, and it is currently employed in the study of thermal degradation of different materials [18, 19].

Optical observations of thermal events during DSC measurements can be very useful for understanding these events [20, 21]. Thus, in order to contribute to a better understanding of the physicochemical and spectroscopic properties of sulindac in polymorphic form II, which is the most common commercial form, we carried out the study of this drug by simultaneous thermogravimetry–differential scanning calorimetry (TG–DSC) coupled to MIR evolved gas analyses (TG-EGA-MIR), and differential scanning calorimetry coupled to an optical microscopy system (DSC–optical microscopy).

Materials and methods

Thermal studies

Sulindac (acid form) of ≥99 % purity was obtained from Aldrich in polymorphic form II. Simultaneous TG–DSC curves were obtained using Mettler Toledo thermal analysis equipment, model TGA/DSC Star^{e} System, under the following experimental conditions: open α-alumina crucibles; heating rate of 10 °C min^{-1}; dry air and nitrogen as purge gas at 50 mL min^{-1} flow rate; and sample weighing about 10 mg. The polymorphic form II was confirmed by DSC, MIR, and XRD data when compared to those previously reported [9–11].

Coupled techniques TG-EGA-MIR and DSC–optical microscopy

The analyses of the evolved gaseous products were performed by connecting the exhaust of the TG–DSC equipment to a Nicolet iS10 spectrophotometer (Thermo Scientific) with a gas cell operating at 25 °C and a DTGS (deuterated triglycine sulfate) detector. The coupling was performed using a stainless steel line transfer (length 120 cm, diameter 3 mm) heated to 25 °C and purged with dry air at a 50 mL min^{-1} flow rate. The MIR spectra were recorded with 32 scans per spectrum at a resolution of 4 cm^{-1}.

The DSC curves were obtained using a DSC 1 system (Mettler Toledo) under the following experimental conditions: aluminum crucible with perforated cover; heating rate of 10 °C min^{-1}; air atmosphere at 50 mL min^{-1} flow; and sample of about 3–5 mg. For the optical observations of the thermal events during the DSC measurements, the system was coupled to a 3 Megapixel CMOS Color Camera (SC30, Olympus) and a computer for image acquisition and storage. The experimental conditions during this experiment were the same, but an open α-alumina crucible was used.

Spectroscopic studies

The attenuated total reflectance middle-infrared (MIR) spectra were run on a Nicolet iS10 MIR spectrophotometer using an ATR accessory with Ge window within the 4000–600 cm^{-1} range. The near-infrared spectra (NIR) were collected using a Thermo Scientific Antaris II spectrophotometer by reflectance within the 1000–2500 nm range.

The ultraviolet and visible spectra (UV–Vis) were collected using an Agilent HP 8453 spectrophotometer within the 200–800 nm range; a 2.5×10^{-5} mol L^{-1} ethanolic solution was prepared for this analysis.

The photoluminescence spectra in solid state were collected using a PerkinElmer LS 55 fluorescence spectrometer, and the photoluminescence spectra in solution were collected using a Cary eclipse spectrophotometer; a 5×10^{-6} mol L^{-1} ethanolic solution was prepared for this analysis.

Results and discussion

Thermal studies

The TG/DTG and TG–DSC curves in dry air atmosphere of sulindac are shown in Fig. 2a. At 188 °C, an endothermic peak in the DSC curve was observed that corresponded to the melting temperature of the drug, which started at about 175 °C (T_{onset}); the drug was stable up to 205 °C. It is noteworthy that no significant mass loss was observed before 205 °C, the temperature at which the thermal event associated with the merger ended completely, although the literature [11] states that the compound decomposes along with the merger. However, this was not observed either in the TG–DSC curves or in a laboratory experiment using a melting point apparatus. The anhydrous compound was stable up to about 205 °C, when its thermal decomposition occurred in four stages, in accordance with data from the DTG curves. The first decomposition stage was in the range of 205–308 °C, where an exothermic peak was observed in the DSC curve at about 265 °C, which corresponded to 16.85 % by mass. A subsequent stage took place in the temperature range 308–415 °C with a mass loss of 10.47 %, where an exotherm in the DSC curve was noticed in the temperature range 295–413 °C. The third decomposition stage occurred in the range 415–645 °C and was associated with a high exothermic peak at 565 °C, which resulted from the oxidation of organic matter, equivalent to 71.86 %. The fourth decomposition stage was observed between 645 and 900 °C. This corresponded to a 0.82 % mass loss, which referred to the decomposition of carbonized material. There was insufficient heat for this to be clearly observed in the DSC curve.

The analysis was repeated in a nitrogen atmosphere (Fig. 2b) to investigate whether simultaneously melting and decomposition could occur under other conditions. However, under these conditions the melting of the drug followed by decomposition was also observed. In this case, decomposition occurred in two stages, according to the TG curve, whereas the DTG curve suggested a higher number of consecutive and/or overlapping stages, with the formation of carbonaceous residue (coke) about 40 % by mass. The details of the thermal events (mass losses and temperature intervals and peaks) are described in Table 1.

The heat–cool–heat cyclic DSC curves are shown in Fig. 3. During heating, the melting of the sulindac started at 182 °C (T_{onset}), with a peak temperature at 187 °C and a melting heat ($\Delta_{fus}H$) of 30.51 kJ mol^{-1}, which was in agreement with previous studies [9–11]. The purity of 99.7 % was calculated using the Van't Hoff equation. In the following cooling–heating stages, there was not any event that could be associated with the recrystallization of the drug [22, 23].

During cooling, it was possible to observe a glass transition (T_g) at approximately 90 °C that was represented by a change in the baseline of the DSC curve, which is typical of amorphous compounds. In the second heating stage, there was an endothermic peak at approximately 90 °C that was associated with the reversion of the glass transition of the drug. However, in this case, instead of a change in the baseline in the DSC curve a relaxation peak associated with this event was observed. This relaxation endothermic peak corresponded with what has been previously discussed in the literature regarding other glassy pharmaceuticals, including indomethacin, which is analogous to the drug sulindac [24, 25]. The intensity of the relaxation peak in the glass transition was directly related to the cooling rate of the fused drug, as shown in Fig. 4. The area under the endothermic peak ranged from 4.9 g J^{-1} at a cooling rate of 0.5 °C min^{-1} to 2.6 J g^{-1} at a cooling rate of 5 °C min^{-1}; the relaxation peak was not observed at a cooling rate of 10 °C min^{-1}. Thus, the

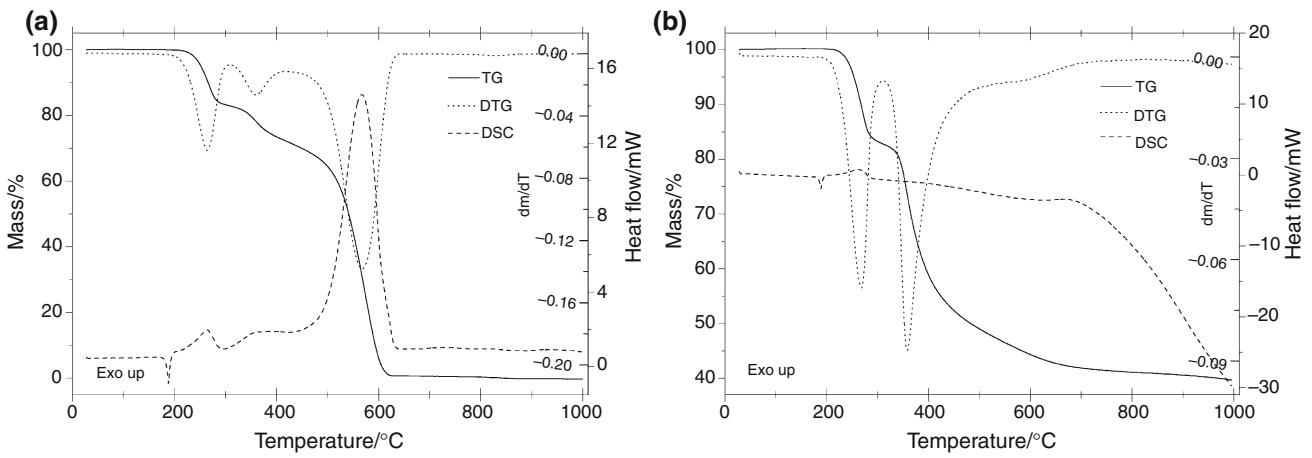

Fig. 2 TG/DTG–DSC curves for sulindac in **a** dry air atmosphere (m = 10.025 mg) and **b** nitrogen atmosphere (m = 10.051 mg)

Table 1 Temperature ranges θ, mass losses, and peak temperatures observed for each step of the TG–DSC curves of sulindac

Atmosphere	Steps			
	First	Second	Third	Fourth
Air				
θ °C	205–308	308–415	415–645	645–900
Loss/%	16.85	10.47	71.86	0.82
Peak/°C	265 (exo)	366 (exo)	565 (exo)	–
Nitrogen				
θ °C	205–310	310–509	509–990	–
Loss/%	16.97	35.01	8.02	–
Peak/°C	263 (exo)	–	610 (endo)	–

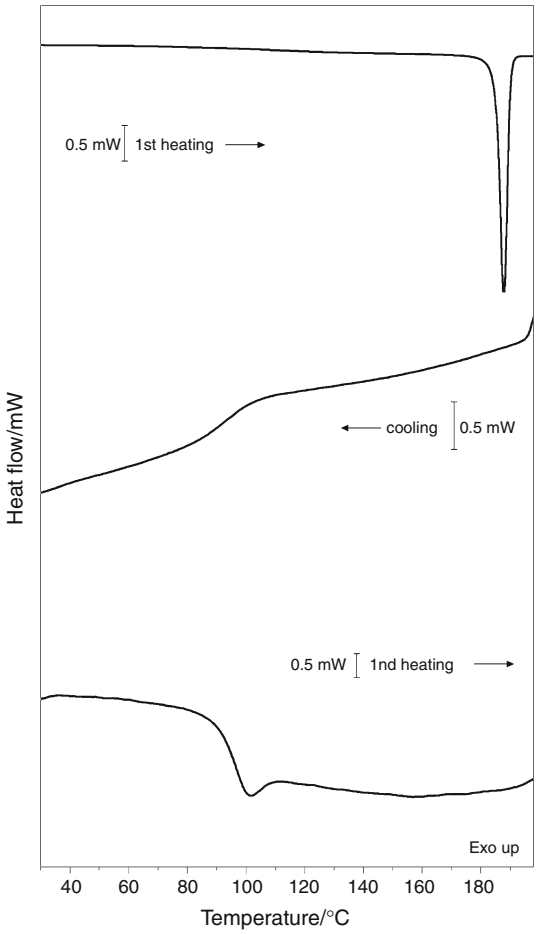

Fig. 3 Heat–cool–heat DSC curves for sulindac ($m = 5.01$ mg)

relaxation peak area increased with the difference between the cooling and heating rate, which reflects the dynamics of the molecular motion freezing [24], something that has already been extensively discussed in the literature [26, 27]. These data are extremely valuable because amorphous drugs generally have a higher dissolution rate than the crystalline form, which consequently leads to greater bioavailability of the drug [28].

The images obtained with the camera during the DSC measurements (Fig. 5) showed the drug melting, followed by the formation of the glassy state. The other thermal events observed in the DSC curves could not be photographed due to the magnification of the camera.

The EGA data provided important information about the volatile compounds that evolved during the thermal decomposition of the sulindac. The study of the degradation products of active ingredients is of utmost importance because they may appear as impurities in the active ingredients [16, 17]. Figure 1S (see supplementary material) shows the infrared spectra in three dimensions that were collected in nitrogen and air atmospheres with a sample mass of approximately 10 mg and a heating rate of 10 °C min^{-1}. These results were in agreement with the observed decomposition stages in the TG–DSC curves.

The spectra obtained above 20 min (>200 °C), shown in Fig. 6a, suggest that the sulindac released formaldehyde in its first stage of decomposition, which was observed in both

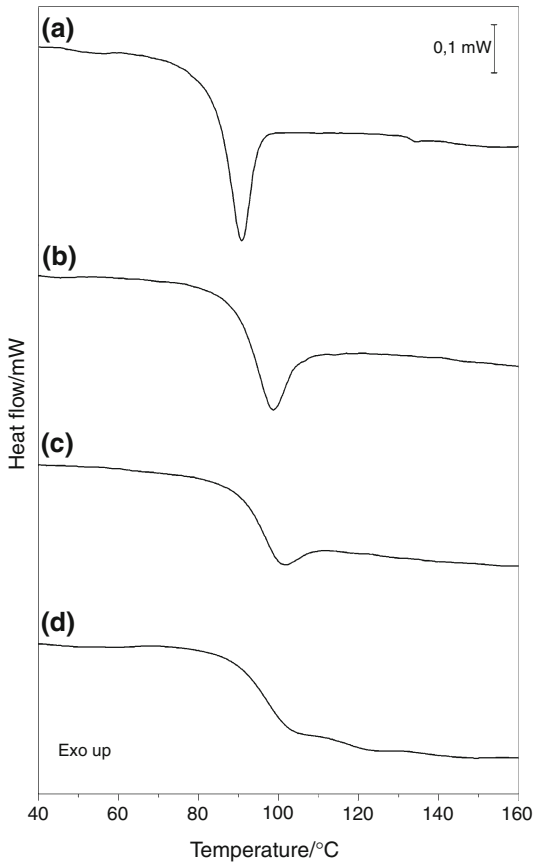

Fig. 4 Heating DSC scans (10 °C min^{-1}) recorded in the glass transition region of molten sulindac cooled at different cooling rates: (*a*) 0.5 °C min^{-1}; (*b*) 1 °C min^{-1}; (*c*) 5 °C min^{-1}; (*d*) 10 °C min^{-1} ($m = 3.01$ mg)

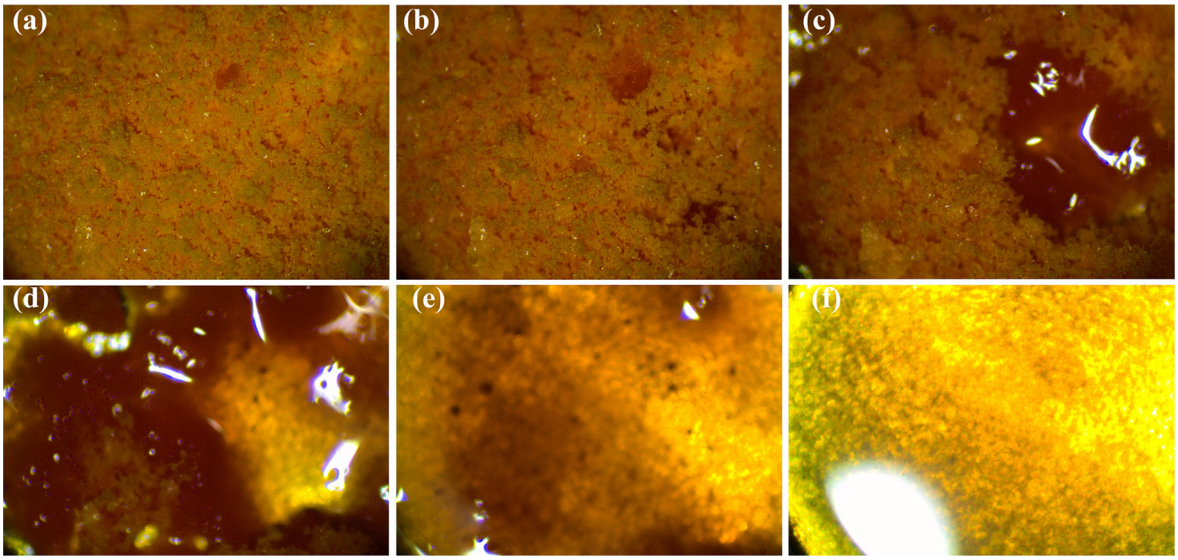

Fig. 5 Images of sulindac obtained at **a** 50 °C; **b** 186 °C; **c** 186.5 °C; **d** 187 °C; **e** 187.5 °C; and **f** 188 °C during melting in DSC measurements

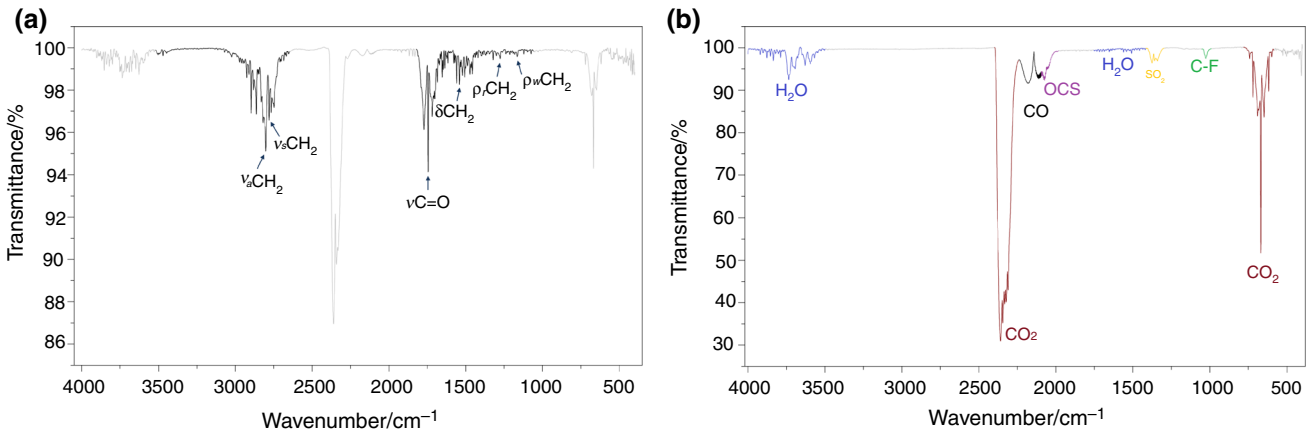

Fig. 6 MIR spectra of volatiles resulting from the thermal decomposition of sulindac: **a** formaldehyde release at 210 °C and **b** volatiles release from the oxidation of organic matter at 550 °C

air and nitrogen atmospheres. The peaks at 2800 and 2779 cm^{-1} can, respectively, be assigned to the axially asymmetric and symmetric stretching of the C–H bond of the methylene group, while the peak at 1745 cm^{-1} corresponds to the axial stretching of the C=O bond. The main characteristics of the spectrum bands are summarized in Table 2.

In the stage that corresponded to the oxidation of organic matter in dry air atmosphere at about 55 min (>550 °C), the spectra of the released gases (Fig. 6b) suggested the release of CO_2, CO, H_2O, and SO_2. There was also a band in the spectra at 1030 cm^{-1} that could be

Table 2 Main bands corresponding to the release of formaldehyde at 210 °C

Assignments	Wavenumber/cm^{-1}
$\nu_a CH_2$	2800
$\nu_s CH_2$	2779
νC=O	1745
δCH_2	1472
$\rho_r CH_2$	1275
$\rho_w CH_2$	1163

ν, stretching; δ, scissoring; ρ_r, rocking; ρ_w, wagging; subscripts *a* and *s* denote asymmetric and symmetric, respectively

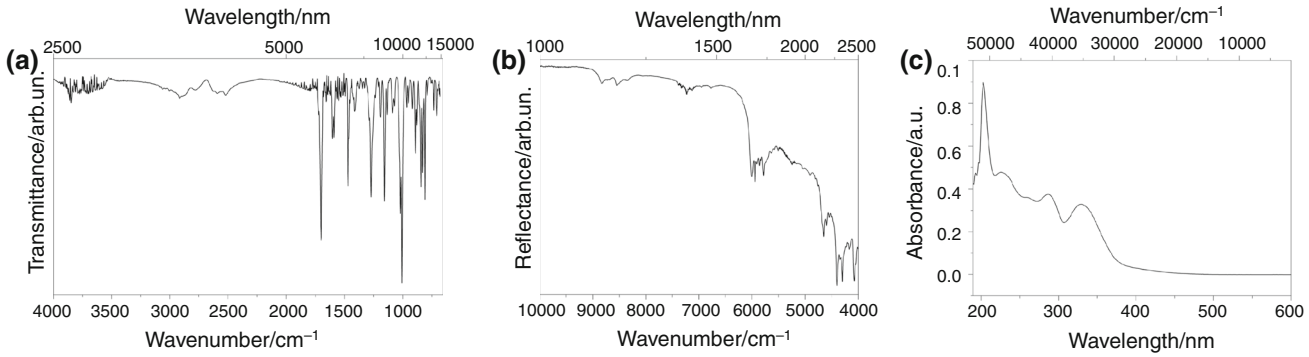

Fig. 7 **a** MIR spectra of sulindac, **b** NIR spectra of sulindac, and **c** UV–Vis spectra of sulindac

Table 3 Near- and middle-infrared spectroscopic data of sulindac

Spectra region	Assignments	Wavenumber/cm^{-1}
Near infrared	$3\nu CH_3$	8825, 8723, 8691
	$3\nu CH_2$	8546, 8506, 8350
	$3\nu CH$	8061
	CH_2 combination bands	7377, 7329
	CH_2 combination bands	7221, 7128
	CH combination bands	6949
	$2\nu OH$	6772
	$2\nu CH_{aromatic}$	6002, 5940
	$2\nu CH_3$	5909, 5860
	$2\nu CH_2$	5832, 5779
	$2\nu CH$	5639, 5577
	$3\nu CO + \nu OH$ combination band	5509
	$3\nu C{=}O$	5239
	OH combination bands	4908, 4805, 4761
	CC combination bands	4649, 4596
	CH_3, CH_2, CH and $CH_{aromatic}$ combination bands	4545, 4508, 4400, 4343, 4298, 4275, 4225, 4172, 4075, 4048
Middle infrared	$1\nu CH_{aromatic}$	3062, 3037, 3003
	$1\nu_a CH_3$	2959
	$1\nu_a CH_2$	2915
	$1\nu_s CH_3$	2892
	$1\nu OH_{dimer}$	2778, 2589, 2521
	$1\nu C{=}O$	1698
	$1\nu C{=}C_{ring}$	1603,1589,1469
	δCH_2	1462
	$\rho_r CH_3$	1453
	δCOH	1413
	δCH_3	1371
	$1\nu C{-}O$	1270
	$1\nu C$-F	1155
	$1\nu S{=}O$	1018,1006
	$\tau HO\cdots H$	842
	ϕ	810
	$\rho_w CH_{ring}$	790
	$\rho_r CH_2$	732

1ν, fundamental stretching; 2ν, first overtone of fundamental stretching; 3ν, second overtone of fundamental stretching; δ, scissoring; ρ_r, rocking; ρ_w, wagging; ϕ, ring breathing; τ, twisting; subscripts *a* and *s* denote asymmetric and symmetric, respectively

assigned to C–F stretching and another at approximately 2070 cm^{-1} that could possibly be attributed to the axial stretching frequency of the carbonyl sulfide (COS), which may have been formed as an intermediate in the reaction between the volatiles (CO and SO_2) that were released during thermal decomposition. These suggestions are consistent with the chemical structure of sulindac.

MIR and NIR studies

The drug was also evaluated by using infrared vibrational spectroscopy. The MIR spectrum of sulindac is shown in Fig. 7a. Sulindac has two methyl groups ($–CH_3$) and one methylene group ($–CH_2$) whose axial deformation absorptions, which corresponded to the symmetric and asymmetric C–H of the CH_2 and CH_3 groups, occurred in the region of 3000–2840 cm^{-1}, overlapping the axial deformation of the O–H band arising from the dimer of the carboxylic acid, which was intense and very broad, and which was observed in the range of 3200–2500 cm^{-1}. The axial deformation band of the carbonyl group (C=O) from the dimer of the carboxylic acid was intense and occurred at approximately 1700 cm^{-1}. This absorption occurred at lower frequencies than expected for a monomer, due to hydrogen bonding and the resonance that weakened the C=O bond.

The NIR spectrum is shown in Fig. 7b. The most important information present in this region was the presence of OH combination bands, especially the one that appeared at 4761 cm^{-1}, confirming the formation of a dimer. The first overtone band of OH appeared at 6772 cm^{-1}, which is a position that is characteristic of the formation of a hydrogen bond.

Table 3 summarizes the main assignments of the MIR and NIR spectrum bands for the infrared of sulindac.

UV and visible regions studies

The UV–Vis spectra are shown in Fig. 7c. Sulindac presented five main absorption bands. The $\lambda_{max} = 203$ nm ($\varepsilon = 35{,}800\ M^{-1}\ cm^{-1}$). The other bands appeared at 227 nm ($\varepsilon = 19{,}000\ M^{-1}\ cm^{-1}$), 261 nm ($\varepsilon = 14{,}360\ M^{-1}\ cm^{-1}$), 287 nm ($\varepsilon = 15{,}000\ M^{-1}\ cm^{-1}$), and 330 nm ($\varepsilon = 13{,}080\ M^{-1}\ cm^{-1}$). A weaker and broader band appeared in the violet region of the visible spectra, which was overlapped by the most intense bands. This absorption gave rise to the yellow color in the compound, in view of the complementarity of yellow and violet colors.

Photoluminescence studies

The solid-state photoluminescence spectra are shown in Fig. 8a. When excited at 240 nm, sulindac showed several emission peaks; the main peaks had their maximum emissions at 390, 485, 532, 602, and 758 nm. The most intense of these was the peak at 390 nm. The photoluminescence spectra for the ethanolic solution are shown in Fig. 8b. The spectra showed the same emission peaks as in the solid state, but a blue shift and a narrowing occurred in all the peaks.

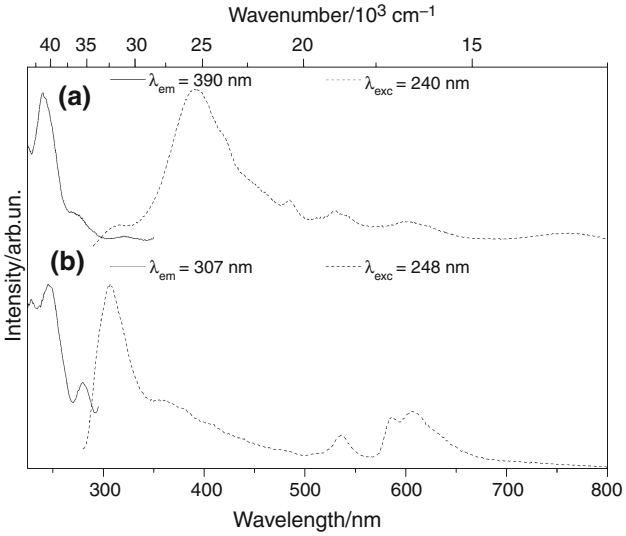

Fig. 8 (*a*) Solid-state excitation and emission spectra and (*b*) ethanolic solution excitation and emission spectra of sulindac

Conclusions

The TG–DSC curves supplied information about the thermal stability and thermal decomposition of sulindac. This non-steroidal anti-inflammatory drug was thermally stable up to 200 °C in air and nitrogen atmosphere and decomposed after melting. The DSC curves showed an endothermic peak at 186 °C that was related to the melting of the sample which did not crystalize again in the heat–cool–heat cycles, resulting in a glassy drug. The information provided by the coupled TG-EGA-MIR techniques suggests that formaldehyde was released during the first stage of thermal decomposition of this compound. These data are of great importance since the products resulting from thermal decomposition can appear as impurities in the active pharmaceutical product. The MIR and NIR spectra provided information about the functional groups present in the sulindac. The UV–Vis spectra provided information about the absorptions that were present and the color of the compound. When the sulindac was excited at 240 nm (in the solid state) and 248 nm (ethanolic solution), several emission peaks were seen, the most intense of which was at 390 nm.

Acknowledgements The authors would like to thank the FAPESP (Proc. 2012/21450-1, 2011/03129-9 and 2013/04096-2) and CNPq foundations (Brazil) for their financial support.

References

1. Shen TY, Witzel BE, Jones H, Linn BO, McPherson J, Greenwald R, Fordice M, Jacob A. Synthesis of a new anti-inflammatory agent, cis-5-fluoro-2-methyl-1-[p-(methylsulfinyl)benzylidenyl]-indene-3-acetic acid. Fed Proc. 1972;31:577.
2. Lenik J. Preparation and characterization of a sulindac sensor based on PVC/TOA-SUL membrane. Mater Sci Eng C. 2014;37:383–9.
3. Lazzaroni M, Porro GB. Gastrointestinal side-effects of traditional non-steroidal anti-inflammatory drugs and new formulations. Aliment Pharmacol Ther. 2004;20:48–58.
4. Shiff SJ, Qiao L, Tsai LL, Rigas B. Sulindac sulfide, an aspirin-like compound, inhibits proliferation, causes cell cycle quiescence, and induces apoptosis in HT-29 colon adenocarcinoma cells. J Clin Investig. 1995;96:491–503.
5. Castonguay A, Rioux N. Inhibition of lung tumourigenesis by sulindac: comparison of two experimental protocols. Carcinogenesis. 1997;18:491–6.
6. Scheper MA, Nikitakis NG, Chaisuparat R, Montaner S, Sauk JJ. Sulindac induces apoptosis and inhibits tumor growth in vivo in head and neck squamous cell carcinoma. Neoplasia. 2007;9:192–9.
7. Wang GH, Jiang FQ, Duan YH, Zeng ZP, Chen F, Dai Y, Chen JB, Liu JX, Liu J, Zhou H, Chen HF, Zeng JZ, Su Y, Yao XS, Zhang XK. Targeting truncated retinoid X receptor-α by CF31 induces TNF-α-dependent apoptosis. Cancer Res. 2013;73:307–18.
8. Coray TW. Inflammation in Alzheimer disease: Driving force, bystander or beneficial response? Nat Med. 2006;12:1005–15.
9. Tros de Ilarduya MC, Martín C, Goñi MM, Martínez-Ohárriz MC. Polymorphism of sulindac: isolation and characterization of a new polymorph and three new solvates. J Pharm Sci. 1997;86:248–51.
10. Grzesiak AL, Matzger AJ. New form discovery for the analgesics flurbiprofen and sulindac facilitated by polymer-induced heteronucleation. J Pharm Sci. 2007;96:2978–86.
11. Plakogiannis FM, McCauley JA. Sulindac. In: Florey K, editor. Analytical profiles of drug substances 13. London: Academic Press; 1984. p. 573–96.
12. Alves GMC, Rolim LA, Neto PJR, Leite ACL, Brondani DJ, Medeiros FPM, Bieber LW, Mendoça Junior FJB. Purificação e caracterização da β-lapachona e estudo de estabilidade dos cristais em diferentes condições de armazenamento. Quím Nova. 2008;31:413–16.
13. Tita D, Jurca T, Fulias A, Marian E, Tita B. Compatibility study of the acetylsalicylic acid with different solid dosage forms excipients. J Therm Anal Calorim. 2013;112:407–19.
14. Tiţa B, Marian E, Fuliaş A, Jurca T, Tiţa D. Thermal stability of piroxicam. Part 2. Kinetic study of the active substance under isothermal conditions. J Therm Anal Calorim. 2013;112:367–74.
15. Hayes JA, Eccles KS, Elcoate CJ, Daly CA, Lawrence SE, Moynihan HA. Crystal polymorphism of methyl 2,3,4-tri-O-acetyl-1-O-(trichloroacetimidoyl)-α-D-glucopyranouronate. J Chem Crystallogr. 2013;43:138–43.
16. Duda-Seiman C, Vlase T, Vlase G, Duda-Seiman D, Albu P, Doca N. Thermal analysis study of amlodipine as pure compound and in binary mixture. J Therm Anal Calorim. 2011;105:677–83.
17. Bannach G, Cervini P, Cavalheiro ETG, Ionashiro M. Using thermal and spectroscopic data to investigate the thermal behavior of epinephrine. Thermochim Acta. 2010;499:123–7.
18. Gálico DA, Holanda BBC, Guerra RB, Legendre AO, Rinaldo D, Treu-Filho O, Bannach G. Thermal and spectroscopic studies on solid ibuprofen of lighter trivalent lanthanides. Thermochim Acta. 2014;575:226–32.
19. Silva ACM, Gálico DA, Guerra RB, Legendre AO, Rinaldo D, Galhiane MS, Bannach G. Study of some volatile compounds evolved from the thermal decomposition of atenolol. J Therm Anal Calorim. 2014;115:2517–20.
20. Perpétuo GL, Gálico DA, Fugita RA, Castro RAE, Eusébio MES, Treu-Filho O, Silva ACM, Bannach G. Thermal behavior of some antihistamines. J Therm Anal Calorim. 2013;111:2019–28.
21. Gálico DA, Perpétuo GL, Castro RAE, Treu-Filho O, Legendre AO, Galhiane MS, Bannach G. Thermoanalytical study of nimesulide and their recrystallization products obtained from solutions of several alcohols. J Therm Anal Calorim. 2014;115:2385–90.
22. ASTM E 928-03 Standard Test Method for Purity by Differential Scanning Calorimetry (2003).
23. Cassel RB. Purity Determination and DSC Tzero technology, TA Instruments Internal Publication TA295a (2002).
24. Kerč J, Srčič S. Thermal analysis of glassy pharmaceuticals. Thermochim Acta. 1995;248:81–95.
25. Descamps M, Aumelas A, Desprez S, Willart JF. The amorphous state of pharmaceuticals obtained or transformed by milling: Sub-Tg features and rejuvenation. J Non-Cryst Solids. 2015;407:72–80.
26. Craig DQM, Royall PG, Kett VL, Hopton ML. The relevance of the amorphous state to pharmaceutical dosage forms: glassy drugs and freeze dried systems. Int J Pharm. 1999;179:179–207.
27. Moynihan CT, Esteal AJ, Wilder J. Dependence of the glass transition temperature on heating and cooling rate. J Phys Chem. 1974;78:2673–7.
28. Carpentier L, Decressain R, De Gusseme A, Neves C, Descamps M. Molecular mobility in glass forming fananserine: a dielectric, NMR, and TMDSC investigation. Pharm Res. 2006;23:798–805.